Title	Ru passivated and Ru doped e-TaN surfaces as combined barrier and liner material for copper interconnects: a first principles study
Authors	Kondati Natarajan, Suresh;Nies, Cara-Lena;Nolan, Michael
Publication date	2019-05-21
Original Citation	Kondati Natarajan, S., Nies, C.-L. and Nolan, M. (2019) 'Ru passivated and Ru doped e-TaN surfaces as combined barrier and liner material for copper interconnects: a first principles study', Journal of Materials Chemistry C, 7(26), pp. 7959-7973. doi: 10.1039/C8TC06118A
Type of publication	Article (peer-reviewed)
Link to publisher's version	10.1039/C8TC06118A
Rights	© 2019, the Authors. Published by the Royal Society of Chemistry. All rights reserved.
Download date	2025-08-03 01:45:17
Item downloaded from	https://hdl.handle.net/10468/8212

Ru Passivated and Ru Doped ε-TaN surfaces as Combined Barrier and Liner Material for Copper Interconnects: A First Principles Study

Suresh Kondati Natarajan*, Cara-Lena Nies* and Michael Nolan

The reduction of the critical dimensions in transistor scaling means that a severe bottleneck arises at the lowest levels of device interconnects. Copper is currently used as the interconnect metal, but requires separate barrier and liner layers, to prevent Cu diffusion and to promote Cu deposition, respectively. Advanced interconnect technology will require coating of very high aspect ratio trench structures which means that the copper barrier/liner stack should take up only a very small volume of the trench to maintain low copper resistivity. The current industry standard for Cu diffusion barrier and liner is TaN and Ru. In this paper we use first principles density functional theory (DFT) computations to explore in detail the interaction of Cu atoms at models of TaN, Ru and combined TaN/Ru barrier/liner materials. This model allows us to explore the role of these materials in Cu adsorption and diffusion (over the surface and into the bulk) in the very early stage of Cu film growth. As a benchmark we studied the behaviour of Cu and Ru adatoms at the low index surfaces of ε-TaN, and the interaction of Cu adatoms with the (0 0 1) surface of hexagonal Ru. These results confirm the barrier and liner properties of TaN and Ru, respectively, while also highlighting the weaknesses of both materials. We then investigate the adsorption and diffusion of Cu adatoms at Ru-passivated and Ru-doped ε-TaN(1 1 0) surfaces. Ru passivated TaN enhances the binding of Cu adatoms compared to the bare TaN and Ru surfaces. On the other hand, the activation energy for Cu diffusion at the Ru passivated TaN surface is lower than on the bare TaN surface which may promote Cu agglomeration. For Ru-doped TaN we find enhanced Cu binding. In addition, we find favourable migration of the Cu adatoms towards the Ru sites, compared with unfavourable migration of Cu away from Ru. This suggests that Ru sites in the TaN surface can act as nucleation points for Cu growth with high activation energies for agglomeration to promote electroplating of Cu. Therefore we propose Ru-doped TaN as a candidate for a combined barrier/liner material which will have reduced thickness compared to individual barrier/liner material stacks.

1 Introduction

Within the semiconductor industry, scaling of interconnects is the most significant limiting factor in the scaling of CMOS transistors.[1,2] In 1997, the replacement of Al with Cu for interconnects overcame some of the issues identified in the International Technology Roadmap for Semiconductors (ITRS) for several technological nodes. However this change has introduced other issues.[3,4]

These include electromigration, which has detrimental effects on device lifetime, as well as the diffusion of Cu into the dielectric.[4] While these issues were also overcome with the use of barrier materials such as Ta and TaN, they are resurfacing as downscaling of devices is set to continue beyond the 5nm node.[4–6] Other problems such as increased Cu resistivity and finding materials that promote Cu electroplating have also been encountered.[4,7]

The original diffusion barriers for Cu interconnects were Ta and Si_3N_4.[6] Since then, a large number of materials have been studied in order to improve device performance and to drive scaling.[8,9] Kaloyeros and Eisenbraun[10] identified refractory transition metals, as well as their binary and ternary systems, as the most promising candidates for Cu diffusion barriers, due to their very high melting temperatures. For compounds with melting tempera-

University College Cork, Tyndall National Institute, Lee Maltings, Dyke Parade, Cork, T12 R5CP, Ireland. Tel: +353 21 234 6983; E-mail: michael.nolan@tyndall.ie
*Authors contributed equally to the manuscript. Author SKN did calculations on the bare TaN surfaces, bare Ru surface and Ru passivated surfaces; Author CLN did calculations on the Ru doped TaN surfaces. † Electronic Supplementary Information (ESI) available. See DOI: 10.1039/b000000x/

tures this high, fast diffusion mechanisms such as grain boundary diffusion become negligible at the operating temperatures of the devices. Grain boundary diffusion has been identified frequently in the literature as the main failure mechanism for Cu diffusion barriers.[9,11] Kaloyeros and Eisenbraun[10] also classified possible diffusion barrier materials into seven groups. The first and second groups comprise pure refractory metals and metal alloys, such as Ta [12], Mo and Os,[13] Ru[14,15] and Ru-Ta alloy.[16] Groups three and four include polycrystalline or amorphous refractory metal nitrides, oxides, carbides, borides and silicates, such as TaN$_x$,[17,18] TiN,[19] and WN$_x$.[11] Some of the more complex materials are included in groups five, six and seven. These are polycrystalline or amorphous silicon nitrides and carbides; amorphous ternary barriers such as TaSiN, WBN and TiSiN; and carbon based compounds such as diamond like carbon coatings. Arguably, 2D materials such as graphene could be added as an eighth group. Graphene has been quite well studied by the research community ever since it was first obtained experimentally.[20] Moreover, there is a growing interest in materials such as MoS$_2$ and graphene as alternative diffusion barrier materials.[21,22]

At present, the semiconductor industry uses a stack of TaN/Ta/Cu. This stack acts as a diffusion barrier to prevent Cu diffusion into the dielectric as well as a Cu adhesion promoter, also referred to as a liner.[23] However, as technology nodes continue to be scaled down to allow greater performance and lower power consumption, a number of issues begin to arise. These include electromigration as well as the increase in Cu resistance. Further, the tri-layer barrier stack becomes difficult to grow via the traditional physical vapour deposition (PVD) methods and while atomic layer deposition (ALD)[24] and atomic layer etch (ALE)[25] have shown promise for film growth at the <5 nm scale, the three layers are still difficult to grow in high aspect ratio vias.[26] This gives rise to the need for alternative, ultrathin barrier materials or a single material that combines all the characteristics of the tri-layer stack.[4,6,23] Many of the refractory transition metal binaries, such as TaN and WN, are poly-crystalline which cause device failure through grain boundary diffusion.[8] It is therefore suggested that amorphous materials would provide better protection against Cu diffusion. By incorporating Si or O into refractory metal nitrides, an amorphous ternary material can be formed, which is suggested to be a more favourable barrier than its binary counterpart.[27] There is however an issue that these amorphous ternary materials have increased resistivity.[8,9]

To our knowledge, the barrier materials mentioned above were mostly studied experimentally to determine the diffusion mechanism and the conditions at which the materials could operate. There have been fewer theoretical studies using density functional theory (DFT) on the use of refractory metals as copper diffusion barriers or their use as liner layers, focusing on a variety of different metals.[28,29] Pure TaN is an excellent barrier for copper diffusion, however it is not well suited for copper electroplating.[7] Nevertheless, when combined with a suitable liner material such as Ru, it has great potential to overcome some of the challenges mentioned above.[28] The phase diagram of TaN determined by Frisk (see section S1 of ESI†) gives an overview of the different solid phase structures of TaN.[30] The δ phase of TaN (fcc lattice)

has been routinely employed in a number of studies in the literature.[18,28] However, the stoichiometric compound ε-TaN with Fe$_2$P crystal structure[31] has the most favourable formation energy. To the best of our knowledge, we found that this hexagonal phase has not been studied in detail computationally when compared to other phases of TaN. The (0 0 1) surface of ε-TaN has been studied previously by Lu and coworkers,[18] where they investigated the interface between Cu(1 1 1) and the TaN(0 0 1) surfaces. However, their study mainly focused on the surfaces of bcc and fcc TaN and they also did not address copper adatom adsorption and mobility at these surfaces. Cheng and co-workers[28] studied the adhesion and mobility of monolayer/bilayer of Cu on N-terminated δ-TaN(1 1 1) and Ru(0 0 1) surfaces as well as monolayers of Cu on Ru passivated N-terminated δ-TaN(1 1 1) surface and predicted Ru as an ideal material for the glue layer that connects the barrier material with the copper wire. However they did not explicitly compute the activation energies for on-surface diffusion, sub-surface diffusion and agglomeration of Ru/Cu adatoms on TaN surface which are important to understand the Cu/Ru nucleation on the TaN surfaces. Therefore, in this paper we examine in detail the low index surfaces of ε-TaN and study the adsorption and diffusion of 1 and 2 Cu/Ru atoms in order to shed light on the mechanism of Cu adsorption, migration and nucleation to better understand Cu growth on barrier and liner films. We want to note that DFT studies of adsorption of metal atoms on oxides has a long history and is of high interest these days in e.g. single metal atom catalysts.[32–42] We study Ru passivated and Ru doped ε-TaN surfaces as they combine the advantages of decreased grain boundary diffusion of ternary materials, the excellent barrier characteristics of TaN and the good liner characteristics of Ru. Ru doped TaN has the potential to be a single barrier+liner material. The main aim of this paper is to find if either or both of these hybrid surfaces could perform effectively as the combined barrier+liner material that would break through the bottleneck in the scaling of copper interconnect technology.

2 Methods and Computational Details

All bulk and surface calculations are performed within DFT using the Vienna Ab initio Simulation Package (VASP) version 5.3.[43] The valence electrons are described explicitly by expanding their wave function in a plane wave basis set with an energy cutoff of 400 eV whereas the core electrons are treated by projector augmented wave (PAW) potentials.[44,45] The valence electronic configurations of the Ta, N, Ru and Cu atoms used in these calculations are 6s^{2}5d^3, 2s^{2}2p^3, 4d^{7}5s^1 and 3d^{10}4s^1, respectively. The DFT calculations are based on spin polarized generalized gradient approximation (GGA) using Perdew-Burke-Ernzerhof (PBE) exchange-correlation functional.[46] The activation energies reported in this paper are computed using climbing image nudged elastic band (CI-NEB) method with 5 images including the starting and ending geometries (3 images only for very short hops).[47,48] The forces acting on the unconstrained atoms in the geometry relaxation calculations as well as the NEB forces in the activation energy computation are converged to 0.02 eV/Å.

The bulk structure of ε-TaN with Fe$_2$P crystal structure is chosen from the Materials Project database[49] and the geometry is
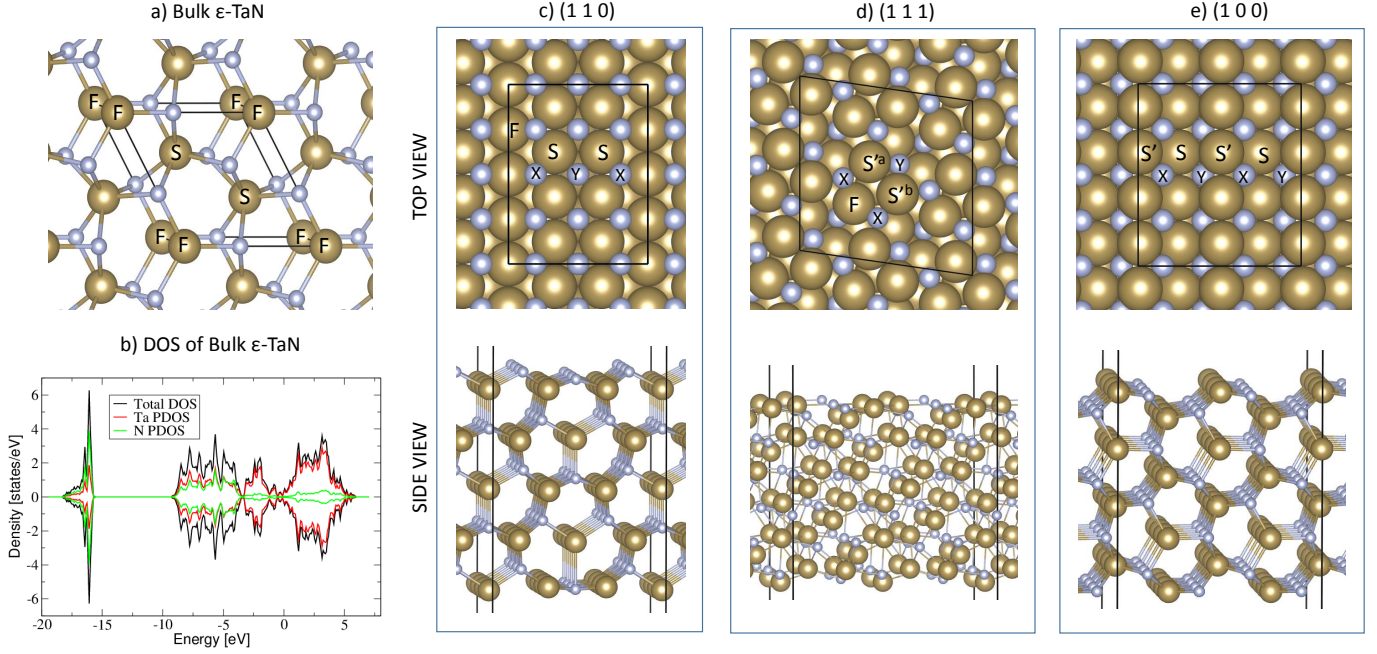
Fig. 1 Panel a) shows the bulk geometry of ε-TaN and panel b) shows the total (black line) and partial density of states (Ta in red and N in green) of ε-TaN where 0 eV in x-axis marks the fermi level. The top and side views of (1 1 0), (1 1 1) and (1 0 0) surfaces of ε-TaN are given in panels c), d) and e), respectively. The Ta and N atoms are shown in ochre and light blue, respectively. The (1 1 0) surface consists of F and S type Ta atoms with valence charges (Q) of 3.6 and 3.0, respectively and N atoms with Q=6.3 (X) and Q=6.4 (Y). Valence charges are computed with respect to total charge density using the Bader code from Henkelman's group.[50,51] On the (1 1 1) surface, we have the S type Ta atoms coordinated by 4 N atoms only (indicated as S') with Q=3.5 (S'^{a}) and Q=3.6 (S'^{b}), F type Ta atoms with Q=3.7 and N atoms with Q=6.5 (X) or Q=6.4 (Y). On the (1 0 0) surface, we have both S and S' type Ta atoms with Q=3.2 and Q=3.7, respectively and N atoms with Q=6.5 (X) or Q=6.4 (Y).

Table 1 Details of the computation models of the low index surfaces of ε-TaN.

Surface	Supercell	K-points	Surf. Area [nm^2]	Layers	TaN/layer	Slab Thickness [Å]	No. Atoms	E_{Surf} [J/m^2]
(1 1 0)	(1×4)	3×2×1	1.06	5	12	11.8	120	2.6
(1 1 1)	(2×2)	3×3×1	1.42	6	12	10.5	144	2.7
(1 0 0)	(1×4)	2×2×1	1.22	8	8	10.2	128	2.7

optimized by simultaneously relaxing the ionic positions, cell volume and cell shape at a higher plane wave energy cutoff of 550 eV and a Monkhorst-Pack K-point mesh of 6×6×12. From this calculation, we arrive at the following equilibrium lattice parameters: a=b=5.23 Å, c=2.92 Å, $\alpha=\beta=90°$ and $\gamma=120°$. This agrees closely with the experimental results of a=b=5.20 Å and C=2.91 Å.[31] The equilibrium geometry of bulk ε-TaN is shown in Figure 1a.

Here, the Ta atoms marked with label 'F' are 3 fold coordinated by N atoms and the resulting coordination polyhedron of this TaN$_3$ fragment is a planar triangle. Ta atoms marked with label 'S' are 6 fold coordinated by N atoms forming two trigonal pyramids connected by their vertices. All N atoms in this geometry are coordinated by 3 Ta atoms out of which two are 'S' type and one is 'F' type. From bader charge partitioning scheme[50,51] we find that the 'F' Ta atoms have a valence charge of 3.8, the 'S' Ta atoms have a charge of 3.3 and the N atoms have a charge of 6.5. We have used the total charge density of the system including the core charges as the reference to compute the valence charges. Therefore the bonding between Ta and N atoms is of a combined ionic and covalent

character. The electron affinity (EA) values of Ta and N atoms are 0.32 eV and -0.07 eV, respectively. Therefore it is not surprising to see that the Ta atoms were oxidized and N atoms were reduced. The total density of states (TDOS) of ε-TaN and the contributions from Ta and N atoms are shown in Figure 1b. It is clear that there is no band gap present and the valence and conduction bands are dominated by the electronic states of Ta. However, it is also observed that the DOS is significantly reduced in the region between the valence and conduction bands suggesting some resistance to electron flow which makes this material a semi-metal. The cohesive energy of ε-TaN is found to be -1.20 eV/atom with reference to bulk Ta[52] and N$_2$ molecule.

The three low index surfaces ((1 1 1), (1 0 0), (1 1 0)) of ε-TaN are considered for this study as they have the lowest surface energies among the 7 possible low index surfaces (see section S2 of ESI†). The surface models are generated with the help of the Atomic Simulation Environment (ASE) package[53] and the properties of these surfaces are listed in Table 1. 12 Å of vacuum separating the slabs along the surface normal direction is included to avoid interactions between the two surfaces of the slab. Out

of the three surfaces, the (1 1 0) surface was found to have the lowest surface energy followed by the (1 1 1) and (1 0 0) surfaces as shown in Table 1. The top and side views of the equilibrium geometries of the above mentioned low-index surfaces along with the valence charges of the top layer atoms are given in Figure 1c-e. From the valence charges obtained from the Bader charge partitioning scheme, we find that the (1 1 0), (1 0 0) have surface Ta atoms that show different charges (Figure 1). The role of this in the adsorption of Cu and Ru is discussed in the results section. The electron affinity values of Cu and Ru are 1.24 eV and 1.05 eV, respectively, which are much larger than that of Ta and N. Therefore we may expect the Cu and Ru adatoms to be oxidized, Cu more so than Ru, when adsorbed on the TaN surfaces. For the adsorption calculations on the low index surfaces, the bottom two layers of the relaxed slab geometries are constrained in their positions.

Bulk Ru in the hexagonal close packed (HCP) lattice is also chosen for this study and the initial geometry is taken from the Materials Project database.[54] The geometry is relaxed in a similar way to the TaN case with an increased energy cutoff of 550 eV and a dense K-point mesh of $12 \times 12 \times 6$. From this the equilibrium lattice constants are found to be a=b=2.71 Å, c=4.28 Å, $\alpha = \beta = 90°$ and $\gamma = 120°$, which compares well with the experimental results.[55] The cohesive energy per atom with reference to atomic Ru is computed to be -6.81 eV, which also agrees with experiments.[56] The geometry of bulk Ru showing the HCP arrangement is shown in Figure S3a of ESI.†

The total DOS of Ru is plotted in Figure S3b of ESI† which shows its metallic nature. For the Cu adsorption calculations, a 10.5 Å thick, 6 layered Ru(0 0 1) slab with a surface energy of 2.53 J/m^2, as shown in Figures S3c and S3d of ESI†, is chosen and a Monkhorst-Pack K-point mesh of $3 \times 3 \times 1$ is used.

Surface energies reported in this paper are computed as follows:

$$E_{surf} = \frac{1}{2A}(E - (nE_{TaN})). \quad (1)$$

Where, A is the surface area of the supercell, n is the total number of TaN units in the supercell, E_{TaN} is the energy of a unit TaN in bulk and E is the total energy of the surface. Adsorption/binding energies are computed using:

$$E_{bind} = (E_{total} - (E_{surface\,only} + E_{adsorbate\,only})). \quad (2)$$

Where, E_{total} is the total energy of the interacting system (adsorbate atoms bound to the surface), $E_{surface\,only}$ and $E_{adsorbate\,only}$ are the total energies of the bare surface and isolated adsorbate atoms, respectively. Activation energy required by the system to hop from state A to state B is computed using:

$$E_{A-B} = |(E_A - (E_{TS_{AB}}))|. \quad (3)$$

Where, E_A is the energy of state A and $E_{TS_{AB}}$ is the energy of the transition state connecting states A and B that is computed using CI-NEB approach.

3 Results

In this section, we will first investigate the adsorption and diffusion of Ru and Cu adatoms at the most favourable low index surfaces
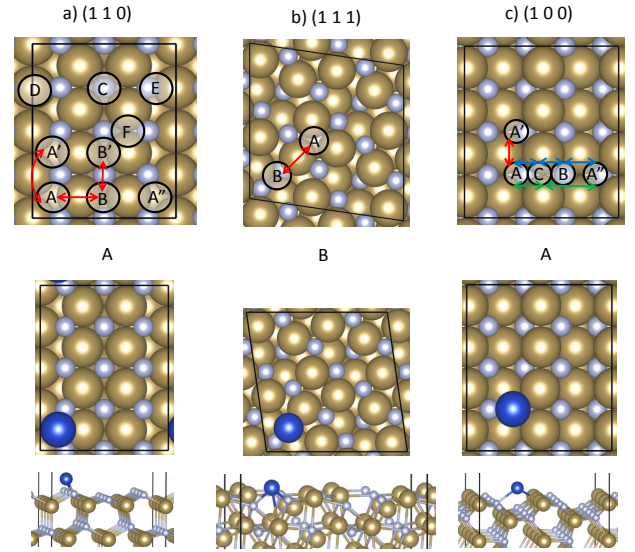

Fig. 2 The low index surfaces of TaN showing the unique binding sites, which are also the end points used for the CI-NEB calculations to compute the activation energies for lateral diffusion of a single adatom. The red arrows indicate pathways for both Ru and Cu adatoms, green arrows are for Cu adatom and blue arrows are for Ru adatom. The Ta and N atoms are shown in ochre and light blue, respectively. The top and side views of the most favourable minimum geometry are also provided for each surface.

of TaN. Following this, similar calculations for Cu adatoms at a hexagonal Ru(0 0 1) slab will be reported. In the next subsection, Ru passivation on TaN and subsequent adsorption and diffusion of Cu atoms will be investigated. Finally, we discuss Ru incorporation into TaN and the interaction with Cu adatoms.

3.1 Ru and Cu Adatoms at Bare ε-TaN Surfaces
3.1.1 1 Adatom Adsorption

Ru and Cu atoms are adsorbed at various unique sites on the most favourable low index ε-TaN surfaces ((1 1 0), (1 1 1) and (1 0 0)) and the stable sites found after relaxation along with schematic pathways connecting them are shown in Figure 2. This figure also includes the top and side views of the most favourable minimum geometries of the respective surfaces. For these geometries, the adatom binding energies, selected interatomic distances (Cu-Ta, Ru-Ta, Cu-N and Ru-N) and bader charge on the adatom are listed in Table 2. The corresponding values for all the computed minima and their geometries are given in section S4.1 of ESI.†

For the (1 1 0) surface, shown in Figure 2a, site A, a 5 fold hollow site coordinated by 3 Ta and 2 N atoms, is the most favourable adsorption site for both Ru and Cu adatoms. At this site, the Ru adatom binds with an energy of -4.95 eV, which is 2.13 eV stronger than that of the Cu adatom. The Cu-N and Ru-N distances are very similar (1.9 Å), but the Ru-Ta distance is about 0.2 Å shorter than the Cu-Ta distance. From the Bader charge analysis we find that both Cu and Ru adatoms are oxidized with net computed Bader charges of 0.5 and 0.2 |e|, respectively (see Table 2). This is due to the electron affinity differences between Cu/Ru and Ta/N. On the (1 1 1) surface, site B, a wide hollow site between a pair of N and Ta atoms, is more favoured by both Ru and Cu adatoms.

Table 2 Binding energies, average distances and valence electronic charge of Cu and Ru adatoms on the low index surfaces of ε-TaN. d(X-Y) gives the average bond length between the neighbouring X and Y species in the corresponding minimum geometries. Q(X) gives the computed charge of atom X according to the Bader charge partitioning scheme.

| Surface	Sites	E_{bind} [eV/ads.]		Interatomic distance [Å]						Q(Cu)	Q(Ru)
		Cu	Ru	Cu-Cu	Ru-Ru	Cu-N	Ru-N	Cu-Ta	Ru-Ta		
				1 Cu/Ru adatom							
(1 1 0)	A	**-2.82**	**-4.95**			1.9	1.9	2.8	2.6	10.5	7.8
(1 1 1)	B	**-3.21**	**-5.64**			2.0	2.0	2.5	2.4	11.2	8.4
(1 0 0)	A	**-3.26**	**-5.67**			2.1	2.1	2.7	2.6	11.1	8.3
				2 Cu/Ru adatom							
(1 1 0)	AA"	**-2.98**	**-5.04**	2.4	2.4	2.0	2.0	2.8	2.8	10.6/10.6	7.7/7.5
(1 1 1)	AB	**-3.04**	-5.37	3.8	4.0	2.5	2.6	2.6	2.4	11.2/11.3	8.4/8.7
	A2B	-2.96	**-5.53**	2.4	2.4	2.0	2.0	2.7	2.6	11.0/11.1	8.3/8.2
(1 0 0)	AA'c	**-3.37**	-5.64	2.7	3.0	2.1	2.0	2.7	2.7	11.0/11.1	8.3/8.2
	AA'a	-3.25	**-5.74**	5.9	5.8	2.1	2.1	2.7	2.7	11.1/11.1	8.3/8.3
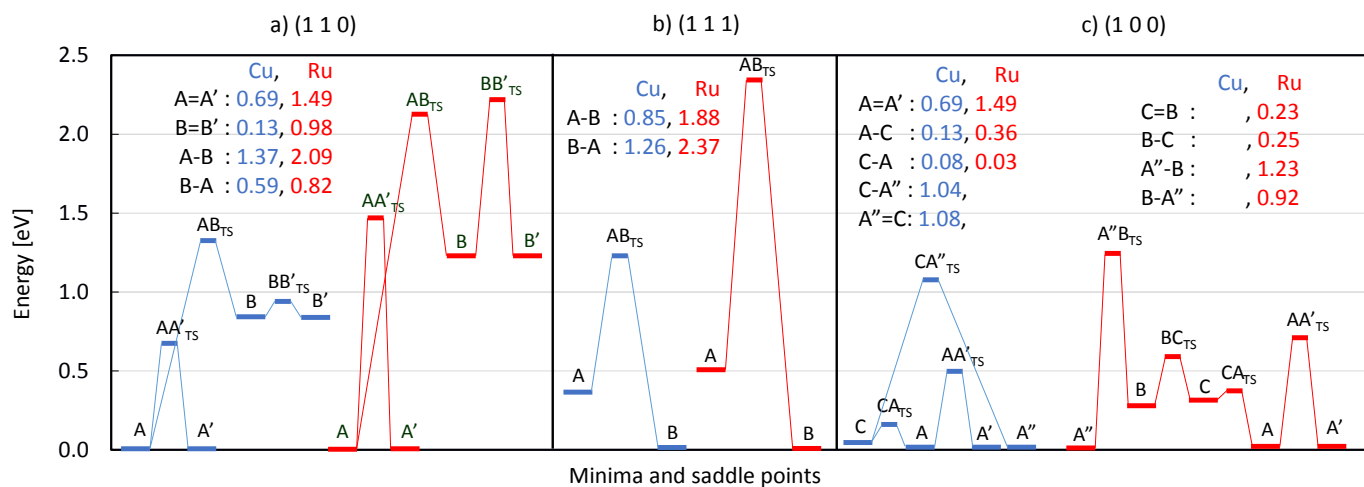
Fig. 3 Panels a), b) and c) shows the saddle points and activation energies for the on-surface hopping of the Cu/Ru adatoms on the (1 1 0), (1 1 1) and (1 0 0) surfaces of ε-TaN, respectively. The numbers and edges in blue correspond to Cu and those in red correspond to Ru.

Similar to the (1 1 0) surface, we find that the Ru adatom binds about -2.43 eV stronger than the Cu adatom. However, in contrast to the (1 1 0) surface we find that both Cu and Ru adatoms are reduced on this surface, Table 2. The adatoms gain electrons from the neighbouring Ta atoms, which are not as oxidized as those in the (1 1 0) surface (see section S5 of ESI† for detailed analysis). On the (1 0 0) surface, site A, a three fold site coordinated by 2 Ta and 1 N atoms, is the lowest energy site for both Ru and Cu adsorption. Similar to the (1 1 1) surface, the Cu and Ru adatoms are partially reduced at this surface as evident from the computed Bader charges reported in Table 2.

As the next step, the activation energies for adatom hops on these surfaces are shown in Figure 3. From the most stable site A on the (1 1 0) surface, the Cu and Ru adatoms can hop to an adjacent identical site along the trench (site A') by overcoming activation energies of 0.69 eV and 1.49 eV, respectively. Similarly, the adatoms can also hop back and forth between sites B and B' by

overcoming just 0.13 eV in the case of Cu and 0.98 eV in the case of Ru. There is a relatively larger activation energy for the adatoms to diffuse from site A to site B (1.37 eV for Cu and 2.09 eV for Ru) when compared to the reverse hop (0.59 eV for Cu and 0.82 eV for Ru) because site A is the most favourable binding site on this surface. The activation energies for hopping are larger for Ru than Cu, which is expected due to the relatively stronger binding of Ru on the (1 1 0) surface as mentioned above. On the (1 1 1) surface, we find that the activation energies for Ru migration from the most favourable site B to site A is about 2.37 eV which is 1.11 eV larger than that of Cu. On the (1 0 0) surface, the activation energy to hop from site A to A' along the trench (red arrow in Figure 2c) is significantly smaller the combined activation energy for a hop across the trench (green arrows for Cu and blue arrows for Ru in Figure 2c). Unlike the (1 1 0) and (1 1 1) surfaces, the activation energies for hops are almost comparable for both Cu and Ru adatoms on the (1 0 0) surface.
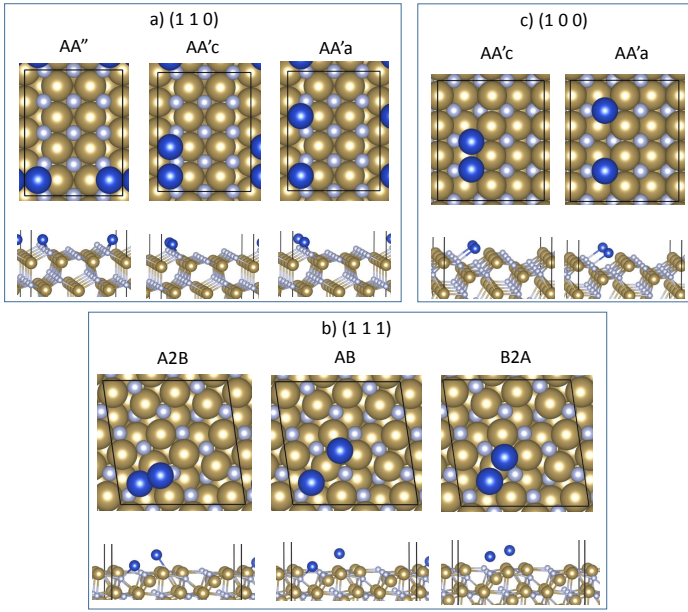
Fig. 4 Most favourable minimum energy geometries of 2 adatoms (Cu/Ru) at the selected low index surfaces of ε-TaN. Here A2B represents the geometry where the adatom at site A moved towards the adatom at site B and vice-versa. AA'c and AA'a represents 2 atom sites where the adatoms are close to each other and distant from each other, respectively. The Ta and N atoms are shown in ochre and light blue, respectively. The adatom (Cu or Ru) is shown in blue.

To summarize, relatively stronger adatom binding is observed on the (1 1 1) and (1 0 0) surfaces of TaN as compared to the (1 1 0) surface. Ru binds significantly stronger than Cu on the TaN surfaces. The lowest activation energies for on-surface diffusion are observed on the (1 0 0) surface followed by the (1 1 0) and (1 1 1) surfaces. We also find that the Ru and Cu adatoms are oxidized on the (1 1 0) surface, while they are reduced on the (1 1 1) and (1 0 0) surfaces. Clearly, the (1 1 0) surface behaves differently from the other two surfaces.

3.1.2 2 Adatom Adsorption

As the next step 2 Cu/Ru adsorption is studied on the most favourable low index surfaces. This is carried out in such a way that the first adatom is placed at the most favourable site on the respective surface and the second adatom is placed at the remaining sites adjacent to the first adatom. The binding energies, selected interatomic distances and adatom charges in the most favourable minimum geometries are listed in Table 2 and the corresponding geometries are shown in Figure 4. This figure also includes the geometries (AA'a and AA'c) that are used to compute activation energies of association. AA'c and AA'a refer to geometries where A' is adjacent to A and A' is away from A, respectively. The energies and geometries of the other minima are discussed in section S4.2 of ESI.†

On the (1 1 0) surface, the most favourable binding is observed when the Cu or Ru atoms are adsorbed at sites A and A" (AA") which are located adjacent to each other on the (1×4) supercell of TaN (1 1 0) surface (see Figure 4a). Comparing the results of the 2 adatom case with the 1 adatom case, we do not find a signifi-

cant increase in the binding energies per Cu/Ru atom even though the two adatoms are close to each other. Therefore the adatom-adatom interaction must be small. Similar to the 1 adatom case, the Ru and Cu adatoms are oxidized at all sites on this surface. On the (1 1 1) surface the two adatoms are first adsorbed at sites A and B (AB) to represent the separated state. To examine the association of the adatoms to form Cu-Cu/Ru-Ru bonds, two geometries are constructed by keeping one of the adatoms at either site A or B and the other immediately next to it (A2B and B2A in Figure 4). It appears that Cu adatoms prefer to stay separated (AB is more stable than A2B) while the Ru adatoms prefer to associate close to site B (A2B more stable than AB). On the (1 0 0) surface, the associated state AA'c is the most favourable 2 atom site for Cu adatoms whereas the separated state AA'a is the most favourable for Ru adatoms. Similar to the 1 adatom case, the adatoms at (1 1 1) and (1 0 0) surfaces are moderately reduced or remain neutral.

We have computed the activation energies for adatom association at these surfaces. For (1 1 0) and (1 0 0) surfaces, the migration of the adatom at site A' from AA'a to AA'c could be regarded as adatom association. For the (1 1 1) surface this will be the migration of adatom at site A towards the adatom at site B (AB to A2B) or vice-versa (AB to B2A). On the (1 1 0) surface, Cu prefers the separated state (AA'a) while the Ru prefers the associated state (AA'c). When initialized from the separated state (AA'a), activation energies of about 0.73 eV and 1.32 eV are needed to reach the associated state. For Cu and Ru, the reverse process requires energies of about 0.57 eV and 1.60 eV. On the (1 1 1) surface, while Cu adatoms prefer the separated state, the activation energy needed for them to associate is just 0.16 eV. While Ru adatoms prefer the associated state, the activation energy to separate is 0.47 eV. In contrast to the (1 1 0) surface, the Cu and Ru adatoms on the (1 0 0) surface prefer the associated and separated states, respectively. Activation energies of 0.48 and 0.64 eV are required for the Cu and Ru adatoms to associate on this surface.

To summarize, similar to the 1 adatom case, the adatoms bind more strongly on the (1 0 0) and (1 1 1) surfaces as compared to the (1 1 0) surface. Further, the adatoms are either metallic or slightly reduced on the (1 1 1) and (1 0 0) surface while they are oxidized on the (1 1 0) surface due to the different numbers of F- and S-type Ta atoms on these surfaces. The Cu adatoms at (1 1 0) surface prefer to stay separated and offer the highest activation energy towards association when compared with the other surfaces. Therefore, Cu atoms may wet on the (1 1 0) surface as compared to the other low-index surfaces. Thus, we chose to use the (1 1 0) surface for Ru passivation and doping studies.

3.2 Cu at Hexagonal Ruthenium

Before investigating the interaction of Cu at Ru doped and Ru passivated surfaces, we have to understand the interaction between Cu adatoms and the bare Ru surface.

Figure S4a in ESI† shows the bare Ru(0 0 1) surface along with the stable binding sites for Cu adsorption namely A, B and C, where A is a hcp site, B is a hollow site and C is an atop Ru site. The binding energies and valence charge of one Cu adatom at these sites are
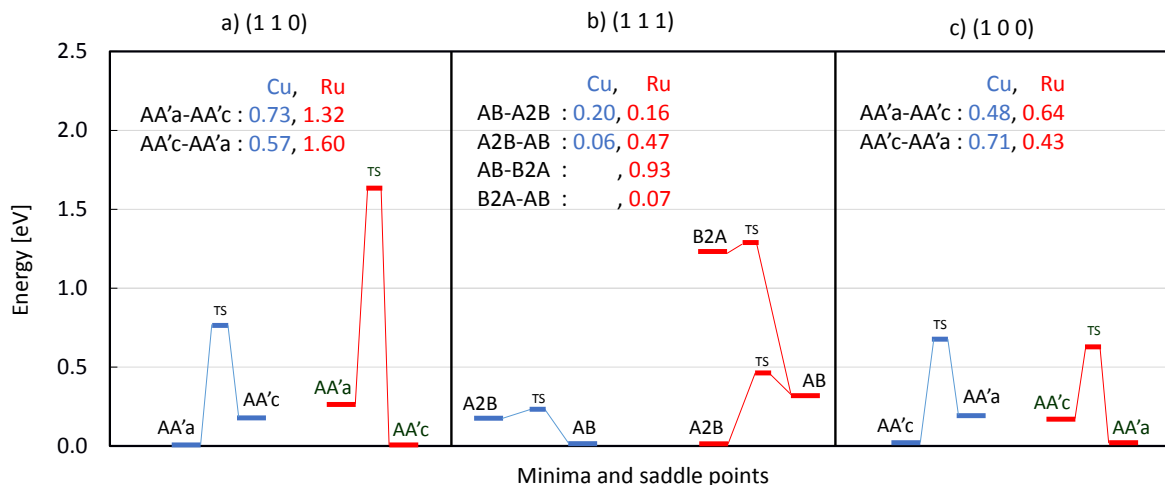
Fig. 5 Panels a), b) and c) shows the saddle points and activation energies for the on-surface association of two Cu/Ru adatoms on the (1 1 0), (1 1 1) and (1 0 0) surfaces of ε-TaN, respectively. The numbers and edges in blue correspond to Cu and those in red correspond to Ru.

Table 3 Binding energies of Cu adatoms on the (0 0 1) surface of Ru.

Sites	Q(Cu)	E_{bind} [eV]
	1 Cu adsorption	
A (HCP)	10.9	-3.18
B (HOLLOW)	10.9	-3.14
C (ATOP)	-	-
A_{exch}	10.9	-2.07
B_{exch}	11.0	-1.52
	2 Cu adsorption	
AAc	10.9/10.9	-3.26
AAa	10.9/10.9	-3.16
BBc	10.9/10.9	-3.22
BBa	10.9/10.9	-3.11

given in Table 3. Adsorption of Cu adatoms on Ru(0 0 1) surface has been studied previously by Qu and co-workers [29,57] using DFT and ultrasoft pseudopotentials. However, they did not compute the hopping/association activation energy or sub-surface diffusion activation energy of the adatoms, which we have focused on in this section.

We have also included the geometries where the Cu adatom from a hcp and a hollow site is exchanged with a surface Ru atom labelled as A_{exch} and B_{exch}, respectively. The Cu atom was not stable at the atop Ru site. The Cu adatom binds with similar binding energies at sites A and B in the range of -3.14 eV to -3.18 eV which is comparable to the TaN surfaces discussed earlier. However, the binding energy decreases considerably (-1.52 to -2.07 eV) when the Cu atom is exchanged with a surface Ru atom. The Cu adatom remains metallic on the Ru surface. The activation energies involved in the on-surface hop and sub-surface exchange of Cu adatoms are given in Figure 6 and the minimum geometries used in the corresponding CI-NEB calculations can be seen in Figure S4b of ESI.† We find that the activation energy for facile diffusion of a Cu adatom on Ru(0 0 1) is in general very small. The activation energy to hop from a hcp to a hollow site (A to B) is only 0.11 eV and the reverse hop is just 0.07 eV supporting the fact that the

hcp site is slightly more preferred by the Cu adatom. In contrast, the activation energy for the exchange process is very large. The activation energy to exchange from a hcp site is about 3.07 eV and from a hollow site is 2.89 eV. The reverse exchange processes have relatively smaller activation energies which are about 1.97 eV for the hcp site and 1.27 eV for the hollow site. In any case, these exchange processes are unlikely due to the high activation energies impeding them.

In the next step two copper atoms are adsorbed on the Ru(0 0 1) surface and we consider two cases. In the first case, the two copper atoms are bound only to hcp sites (AAa and AAc) and in the second case they are bound only to hollow sites (BBa and BBc). The corresponding geometries used for this study are shown in Figure S4c of ESI† and the energies are listed in Table 3. The geometries at sites AAa and BBa represent cases where the adatoms are separated and those at AAc and BBc are cases where the adatoms are adjacent to each other. The binding energies per adsorbed Cu were found to be very similar in the range of -3.11 eV to -3.26 eV. Therefore, we studied the activation energies separating them as indicated by the arrows in Figure S4c of ESI.† A copper atom can diffuse along the surface via two types of hops - hcp to hollow and hollow to hcp. So to migrate from one hcp site to another the adatom must first hop to a hollow site and then to the hcp destination site which involves crossing two activation barriers. From Figure 6 we find the greatest activation energies for the first hop from the associated states AAc (0.26 eV) and BBc (0.22 eV) and the lowest activation energies for the second hop toward the same states (0.01 eV and 0.05 eV). The Cu adatoms are therefore very mobile on the Ru(0 0 1) surface and prefer to associate.

3.3 Ru Passivated TaN Surfaces

In this section, adsorption and diffusion of Cu adatoms on Ru passivated TaN(1 1 0) surfaces will be studied. A discussion on the adsorption of Ru adatoms that resulted in the formation of a passivated layer is given in section S7 of ESI.† For our purposes, we will perform the Cu adsorption and diffusion calculations on 1 ML
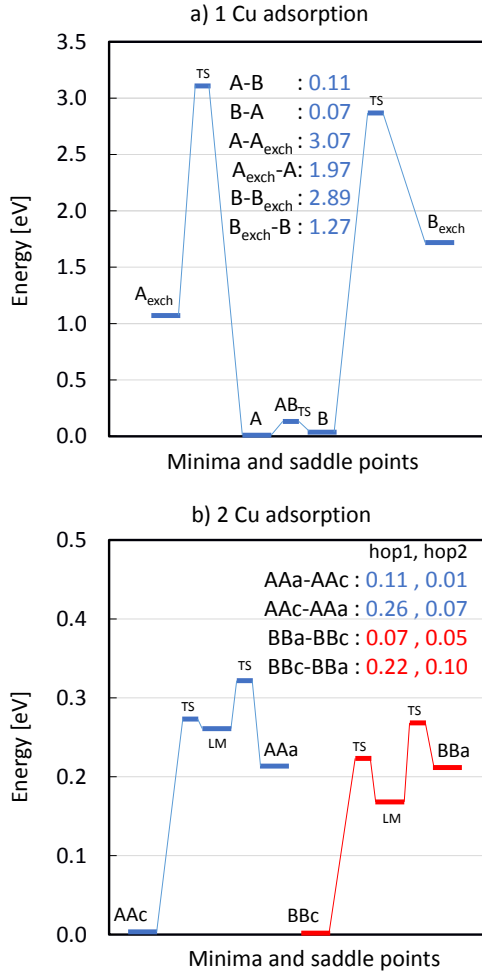
Fig. 6 Panels a) and b) show the minima, saddle points and activation energies for the on-surface diffusion and association of Cu/Ru adatoms on the Ru(0 0 1) surface, respectively. Here, 'LM' refers to local minimum and 'TS' refers to transition state.

Fig. 7 Unique adsorption sites for Cu adsorption on 1 and 2 ML of Ru passivated TaN (1 1 0) surface are shown in panels a and c, respectively. It also includes pathways to compute activation energies for association in two Cu adsorption, where the Cu sites in associated states are highlighted in green and the arrows indicate the pathway. Panels b and d show the geometries where a Cu adatom is adsorbed at sub-surface sites. The Ta, N, Ru and Cu atoms are shown in ochre, light blue, brown and blue, respectively.

and 2 ML of Ru passivated TaN(1 1 0) surfaces (in Figures S11e and S11f of ESI†).

3.3.1 Cu Adatoms at 1 ML Ru passivated TaN(1 1 0) surface

From the three stable binding sites (A, B and C) shown in Figure 7a, the strongest binding is seen at site B, a wide 3 fold site above a sub-surface Ta atom. The binding energies listed in Table 4 are moderately lower than that on the bare (1 1 0) surface suggesting that Ru passivation also promotes Cu binding. We did not find significant changes in the valence charge of the adsorbed Cu atom which indicates that there is no significant electron transfer between the Cu adatom and the Ru layer.

The on-surface hopping activation energies of a Cu adatom between sites A-B and B-C (shown in Figure 8a) are in the range of 0.01 eV - 0.45 eV. The greatest activation energy of 0.45 eV is found for the Cu atom to migrate from site B to site C and the lowest activation energy of 0.01 eV is found for its diffusion from site A to B. These activation energies are comparatively larger than on the bare Ru(0 0 1) surface but smaller than on the bare TaN (1 1 0) surface. We have also looked at the energies of sub-surface ad-
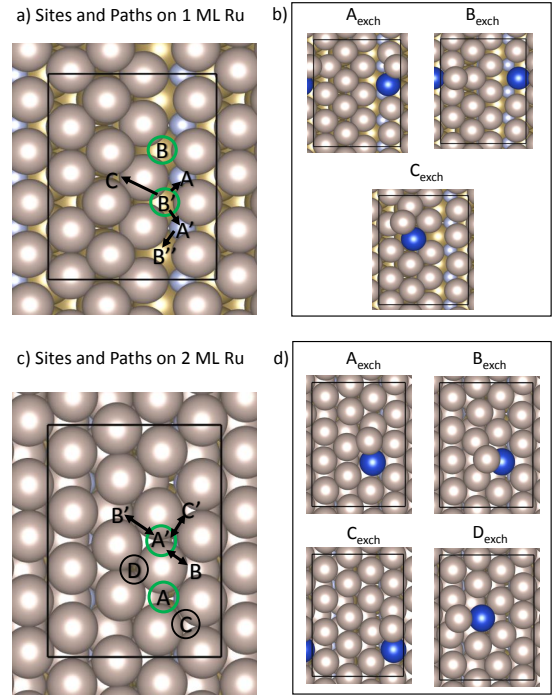
sorption of the Cu adatom from the above mentioned stable sites, as shown in Figure 7b. All the sub-surface adsorption geometries had high energies and large diffusion barriers (see Figure 8a) as compared to the corresponding on-surface adsorption geometries. More on this topic can be found in section S7 of ESI.†

As the next step, adsorption of 2 Cu is investigated where the geometry at site BB' (combined site notation: one adatom at B and the other at B') is found to be the most favourable where the Cu atoms are at a distance of 2.5 Å. Details of the other geometries are discussed in section S7 of ESI.† Compared to the 1 Cu adsorption case, we find that the binding energies have decreased slightly, probably due to the additional Cu-Cu interaction and associated surface rearrangements.

We have chosen the geometry at site BB' as the associated state (shown by green circles in the figure) and computed the activation energies associated with the diffusion of the second Cu atom from site B' to sites A, C and B". The forward activation energies from BB' to the other sites are in the range of 0.35 - 0.48 eV and the reverse activation energies are significantly lower as shown in Figure 8b. This suggests that the Cu adatoms, in addition to diffusing on the surface, prefer to associate more so than on the bare TaN (1 1 0) surface.

3.3.2 Cu Adatoms at 2 ML Ru passivated TaN(1 1 0) surface

On the 2 ML of Ru passivated TaN(1 1 0) surface shown in Figure 7c, the two fold Ru coordinated site A is found to be the most
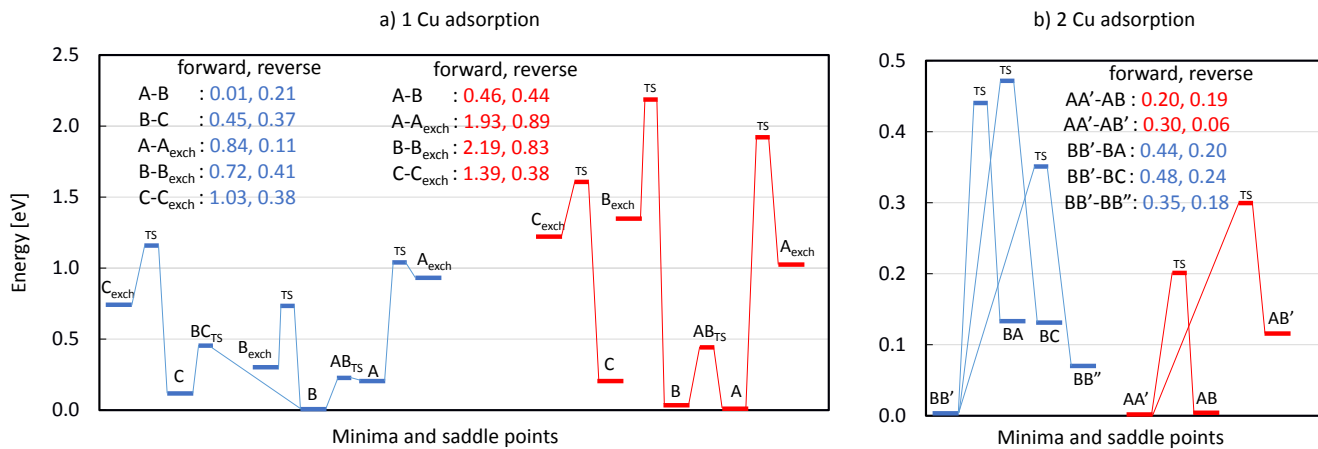
Fig. 8 Panels a) and b) show the minima, saddle points and activation energies for the on-surface/ subsurface diffusion of 1 Cu adatom and association of 2 Cu adatoms on the Ru passivated TaN surfaces, respectively. Here, blue and red colors represent 1 ML and 2 ML of Ru passivated surfaces, respectively.

Table 4 Binding energies and activation energies for the diffusion of Cu adatoms on 1 and 2 ML of Ru passivated TaN (1 1 0) surfaces. A '-' for the E_{bind} indicates that the respective geometry is found to be unstable and a '-' for $E_{activation}$ indicates that we could not find a transition state connecting the minima.

Adatoms	Sites	Q(Cu)	E_{bind} [eV]	d(Cu-Cu) [Å]
		1 ML Ru		
1 Cu	A (3 fold atop N)	10.9	-3.24	
	B (3 fold atop Ta)	11.0	-3.44	
	C (2 fold)	10.9	-3.35	
2 Cu	BB'	11.0/11.0	-3.60	2.5
	BA	11.0/11.0	-3.48	2.6
	BC	11.0/10.9	-3.49	2.9
	BB"	11.0/10.9	-3.52	5.2
		2 ML Ru		
1 Cu	A (2 fold)	11.0	-3.44	
	B (3 fold wide)	11.0	-3.42	
	C (3 fold hcp)	10.9	-3.18	
	D (3 fold hollow)	10.9	-3.13	
2 Cu	AA'	11.0/10.9	-3.43	2.7
	AB	11.0/11.0	-3.43	2.5
	AC	11.0/10.9	-3.35	2.4
	AB'	10.9/11.0	-3.31	4.8
	AC'	11.0/10.9	-3.30	4.6

favourable. Similar to the 1 ML case, there is no significant charge transfer between the Cu and Ru atoms.

The activation energies for the Cu adatom to hop from the most favourable site A to site B is computed to be 0.46 eV and the activation energy for the reverse process is almost the same as shown in Figure 7a. Pathways connecting site A to sites C and D could not be found in our investigation. The sub-surface exchange geometries given in Figure 7d are found to be approximately 1 eV lower in binding energy than the corresponding on-surface adsorption cases. More details can be found in section S7 of ESI.†

For 2 Cu adsorption, the first Cu is placed at site A and the second Cu is placed at sites B, C, A', B' and C' (see Figure 7c). The binding energies per Cu are in the range of -3.30 eV to -3.43 eV

which is comparable to the 1 Cu adsorption energies on this surface.

The association activation energies are computed by keeping the geometry at AA' as the starting point and moving the Cu at A' to sites B, B' and C' as indicated by arrows in Figure 7b. We find that the two atom sites AA' and AB' are equally favourable. For the minimum energy pathways connecting AA' with AB', the forward activation energy is greater than the reverse activation energy indicating a preference for Cu atoms to coordinate with each other.

To summarize, the Cu adatoms bind more strongly at the Ru passivated surfaces as compared to the bare Ru and the bare TaN (1 1 0) surfaces. We also did not observe any significant charge transfer between the Cu and Ru atoms. The on-surface Cu diffusion activation energies are moderately larger than those on bare Ru, but significantly smaller than those on the bare TaN (1 1 0) surface. Therefore, the Cu adatoms are mobile on this surface and might show a preference toward association like they do in the bare Ru surface.

3.4 Ru doped TaN

As an alternative to the Ru passivated surfaces we will now study the Ru doped TaN (1 1 0) surfaces as a single barrier+liner material. All calculations for Cu adsorption on Ru-doped TaN (1 1 0) were carried out using a (2×4) supercell in order to eliminate any finite size effects caused by Ru doping of the (1×4) supercell. However, as will be shown in this section, the effects of Ru in the surface are very localised and thus it is possible to use the smaller (1×4) supercell for the NEB calculations. Although Ru is suitable for copper electroplating, it does not function well, by itself, as a diffusion barrier material. The Ru passivated TaN surfaces studied in the previous section were found to have small activation energies for the on-surface diffusion of copper atoms and may allow Cu association. Therefore the possibility of tuning the TaN surface to allow wetting of Cu through doping with Ru, while retaining the barrier properties of TaN, is the focus of this section. Ta atoms from two surface sites are replaced with Ru as shown in Figure 9a to determine the more favourable doping site.
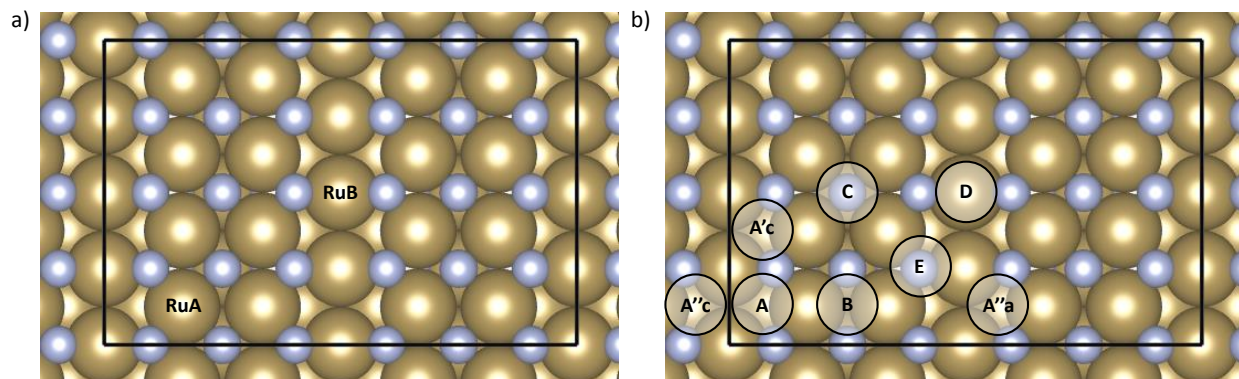
a)

b)

Fig. 9 a) Ru-doping sites and b) Cu adsorption sites on the TaN(1 1 0) surface. The Ta and N atoms are shown in ochre and light blue, respectively.
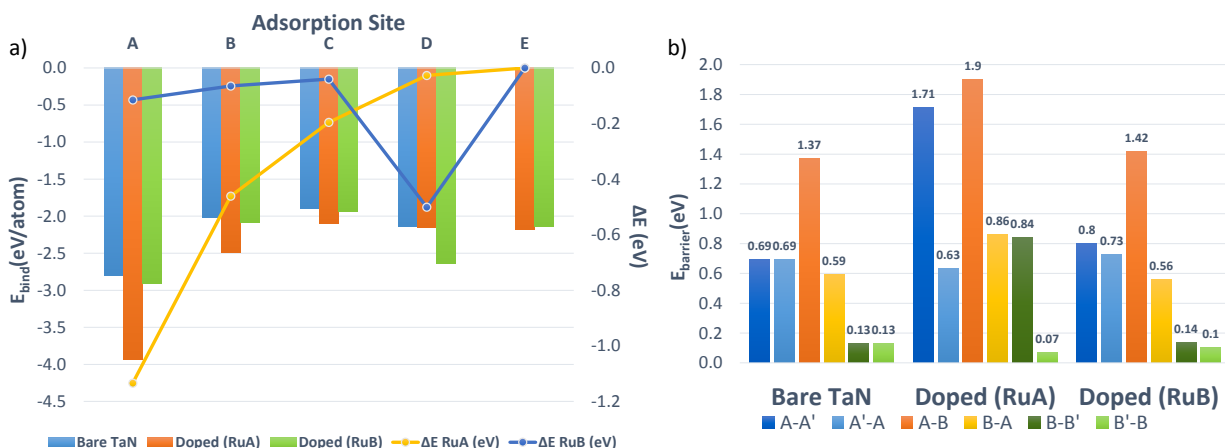
a)

b)

Fig. 10 Comparing changes in a) adsorption energies and b) activation energies between bare (2×4) TaN and Ru-doped (2×4) TaN for each adsorption site.

RuA replaces a surface Ta atom (S type) coordinated to 4 surface N atoms while RuB replaces a surface Ta atom (F type) that is coordinated to 2 surface N atoms. The TaN surface doped with RuB was found to be 2.34 eV more stable than that doped with RuA. Charge analysis of the surface shows that the charges on RuA and RuB are 7.1 and 7.5 respectively. This difference in Ru oxidation is likely the cause of the different surface energies. Details of the surface charges are shown in section S5 of ESI.† The introduction of Ru into the surface did not affect the TaN surface lattice considerably.

3.4.1 1 Adatom Adsorption on Ru-doped TaN(1 1 0)

On the bare (2×4) supercell of the TaN (1 1 0) surface, five unique Cu adsorption sites (A, B, C, D and E) were identified as shown in Figure 9b. The binding energies of a Cu adatom at these five sites on the bare (2×4) surface as well as on the doped surfaces are compared in Figure 10a and the corresponding geometries for the most favourable site on RuA and RuB doped TaN surfaces are given in Figure 11. All other geometries are shown in section S8 of ESI.†

Binding energies for Cu at the different sites range from -2.01 eV to -3.93 eV for the RuA doped surface, from -1.94 eV to -2.92 eV for the RuB doped surface compared to -1.90 eV to -2.80 eV for the bare surface. Overall, site A is the most stable and site C is the least
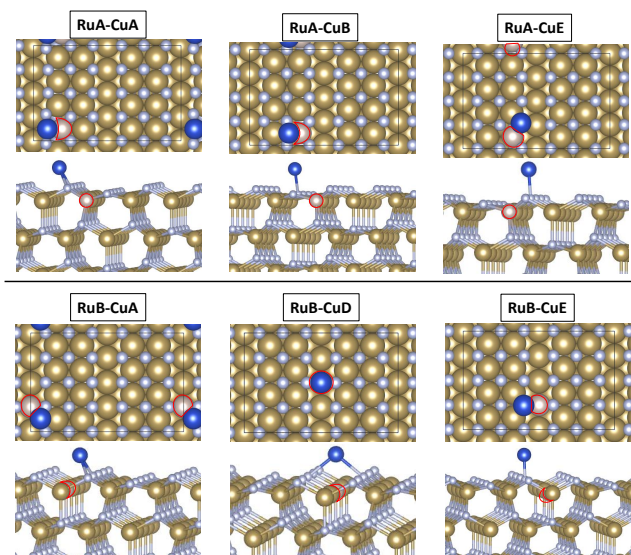

Fig. 11 Adsorption Geometries of most favourable 1 Cu atom on RuA-doped RuB-doped TaN(1 1 0). The Ta, N, Ru and Cu atoms are shown in ochre, light blue, brown and blue, respectively. Ru atoms are highlighted with a red border.
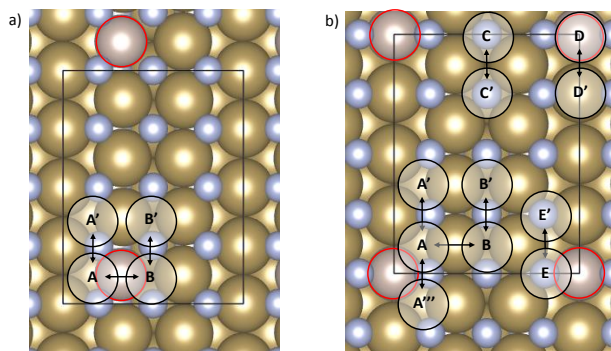
Fig. 12 Migration pathways of Cu adatoms on both doped surfaces a)RuA and b)RuB. The Ta, N, Ru and Cu atoms are shown in ochre, light blue, brown and blue, respectively. Ru atoms are highlighted with a red border.

stable for Cu adsorption on all the three surfaces. It is evident from Figure 10a that the Cu adatom binds slightly more strongly on the Ru doped TaN surfaces as compared to the bare TaN surface. The figure also shows the binding energy difference (ΔE) between the bare and Ru doped surfaces from which the largest change for RuA and RuB doped surfaces is found to have occurred at the sites A (1.13 eV) and D (0.50 eV), respectively. RuA doped surface shows enhanced Cu binding at sites A, B, C and E as compared to RuB doped surface, whereas RuB doped surface shows enhanced Cu binding at site D as compared to RuA doped surface. Therefore, it is clear from the ΔE plot in Figure 10a that those Cu adsorption sites that are closer to the doped Ru atom show enhanced binding as compared to the bare surface. Bader charge analysis showed that the Cu adatom is always oxidized and that the charge of Cu is mostly independent of adsorption site and number of adatoms, although a correlation between binding energies and charge can be observed. The changes in charge are no larger than 0.2 electrons, however atoms that are more oxidised still have a larger binding energy. All Cu charges are shown in Table 5.

To determine how the adsorption of Cu atom affects the surface atomic structure of the Ru doped surfaces, the Ta-N bond lengths near the Cu adsorption sites (Ta-N adsorbed) are compared to those near an equivalent distant site on the same surface (Ta-N distant) and to those near an equivalent site in the bare Ru doped surface (Ta-N bare). The range of distances for these three cases are displayed in Figure S12 of ESI.†. The bond lengths of Ta-N distant are similar to those of Ta-N bare, while the Ta-N bonds near the adsorption sites appear somewhat elongated. However, the changes observed between any of the Ta-N bonds measured across all surfaces, bare and doped, are no more than 0.1-0.2 Å. Therefore, this study shows that in terms of geometry the effect of Cu adsorption and Ru-doping is localised to the adsorption/doping sites.

Due to the localised effect of Ru doping, the CI-NEB calculations were carried out using the smaller (1×4) supercell of TaN (1 1 0). To facilitate this, the minimum geometries and binding energies for 1 Cu adsorption were also computed on the smaller (1×4) supercell and compared with the (2×4) supercell in Table 5. It can be seen that the binding energies are very similar for both supercells supporting the localized effect of Ru doping.

As the next step, the activation energies impeding the migration of a Cu adatom on the Ru doped surfaces were computed. Firstly, we determined the activation energies for migration from the most favourable site (A) to the closest non-equivalent site (B) for both RuA and RuB doped surfaces as shown in Figure 10b and the corresponding pathways in Fig. 12a. On the RuB surface there is only a small increase in the on-surface diffusion activation energies, connecting sites A-A', B-B' and A-B, compared to the bare surface. The large increase in the activation energy for migration for RuA can be attributed to Cu moving across a doped Ru instead of the Ta atom. The activation energies observed on the RuA surface may appear much more favourable compared to those found on the RuB surface, however this is a biased comparison. As the Ru atom is closer to the Cu atom in the adsorption sites A and B on the RuA surface than on the RuB surface, the activation energy will be more affected due to the stronger binding between Cu and Ru compared to Cu and Ta. Therefore the effect of Ru in the surface should be studied on a larger model with a higher percentage of doping, which is beyond the scope of this paper and is the focus of ongoing work.

For our purposes, we studied in detail the migration pathways and the corresponding activation energies on the more favourable RuB surface. The particular migration pathways are shown in Fig. 12b, while the corresponding activation energies are listed in section S8 of ESI† and are also shown in Fig. 9b. The forward and reverse activation energies in the table indicate the activation energies required for the Cu atom to migrate away from and towards the doped Ru, respectively. We observe that it is more favourable for Cu adatom to move towards the doped Ru on the surface than away from it. Especially in the case of migration from site B to A (towards Ru) where the activation energy is almost 2.5 times lower than the migration from A to B (away from Ru). No migration pathways connecting the endpoints C-C', D-D' and E-E' were found. For the migration pathway B-B', very small activation energies of around 0.10 eV were found. The noted exception of this being the activation energy of 0.84 eV required to move a Cu atom away from site B on the RuA surface, where the adatom is directly adjacent to the Ru atom. The activation energy for the exchange of a Cu atom with the doped Ru in the surface is also determined. For Ru to move out of the surface and Cu to take its place the activation energy needed is as high as 3.78 eV. The reverse process has an activation energy of just 1.88 eV. This indicates that Ru doping is unlikely to allow sub-surface Cu adsorption and diffusion which allows the barrier properties of TaN to be maintained.

3.4.2 2 Adatom Adsorption on Ru-doped TaN

In this section we investigate the adsorption of 2 Cu atoms and the activation energy for Cu association on the Ru doped surfaces. The 2 adatom adsorption calculations are done in such a way that the first Cu atom is placed at site A, which is the most favourable site, and the second Cu atom is placed at all the other sites shown in Figure 9b and the geometry is relaxed. Figure 13 shows the geometries for 2 adatoms on the doped surfaces, while Table 5 presents the computed binding energies. The corresponding results from the bare and doped surfaces are listed in Table 5.

As with the single adatom case, the binding energy per adatom

Table 5 Binding Energies of Cu on Ru-doped TaN(1 1 0). Q(Cu) is the charge on the Cu atom adsorbed to a doped surface, where there are two adatoms the charges are separated by a "/"

No. Cu	Ru doping site	Cu adsorption site	E_{bind} [eV]			Q(Cu)
			doped 1x4	doped 2x4	bare 2x4	
1 Cu	RuB	A	-2.88	-2.92	-2.80	10.5
		B	-2.02	-2.09	-2.02	10.5
		C	-1.88	-1.94	-1.90	10.6
		D	-2.56	-2.63	-2.13	10.4
		E	-	-2.14	-	10.5
2 Cu	RuA	AA"c		-3.12	-3.03	10.5/10.6
		AA"a		-3.34	-2.79	10.5/10.5
		AB		-3.21	-2.42	10.6/10.5
		AD		-3.05	-2.42	10.5/10.4
	RuB	AA"c		-3.03	-3.03	10.5/10.6
		AA"a		-2.88	-2.79	10.5/10.5
		AB		-2.51	-2.42	10.5/10.5
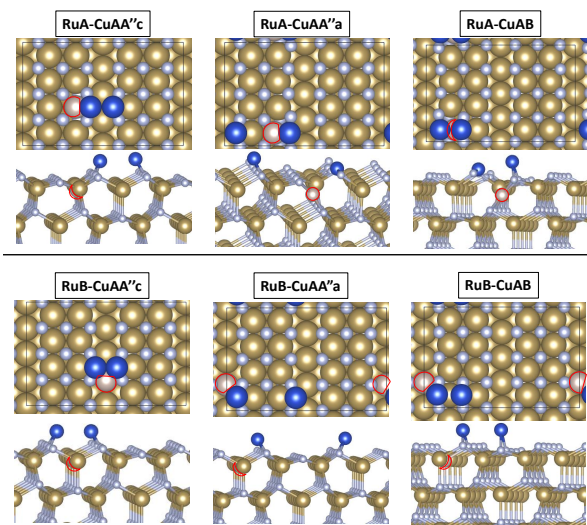
Fig. 13 The most favourable adsorption geometries of 2 Cu atoms on RuA-doped and RuB-doped TaN(1 1 0). The Ta, N, Ru and Cu atoms are shown in ochre, light blue, brown and blue, respectively. Ru atoms are highlighted with a red border.

was enhanced by an average of -0.30 eV when adsorbing 2 Cu atoms on the doped surfaces when compared to the bare surface. On the bare surface, the combination of AC and AE is unstable. The combination of adsorption sites A and E is unstable on the RuA doped surface, while AC is stable. On the RuB-doped surface, AC, AD and AE are all unstable configurations. As the atoms are too far apart on the surface to coordinate, the Cu atom placed at the E site migrates to another A site (the A"a site) on both RuA and RuB doped surfaces. Once the two Cu atoms migrate to the A site, two atoms in adjacent A sites (AA"c) is the most favourable configuration on the RuB-doped surface, with a binding energy of -3.03 eV.

This same AA"c combination has a binding energy of 3.12 eV on the RuA doped surface. Interestingly, this is not the most stable configuration here. Instead with a binding energy of 3.34 eV, it is more favourable for the second Cu atom to adsorb a distant A"a site. In addition to testing Cu adsorption directly on the surface, 2 Cu atoms were adsorbed on top of each other at an A site. When

carrying out this calculation on the bare (1×4) surface and the doped surface, the Cu atoms remain stacked. On the bare (2×4) surface, the top Cu moves off and coordinates at the nearest available A site. This is possibly due to finite supercell size effects.

As for one adatom calculations, the length of bonds between Cu-Ru, Cu-Ta, Cu-N, Ru-Ta and Ru-N were measured for all adsorptions and compared to those measured for the bare surface. Results were consistent with the observations made for the one adatom calculations.

To study association using CI-NEB calculations, 2 Cu atoms were placed at adjacent A sites (AA'c) and the activation energy for one of the atoms to move to the next-nearest A site (AA'a) was computed. On the RuA surface, the activation energy needed to separate the two Cu atoms was 0.70 eV, while the energy to associate was 0.66 eV. On RuB, separation needed 0.60 eV and association needed 0.72 eV. The activation energies for migration are almost symmetrical for RuA, which could be due to competing effects of Cu-Ru interactions and Cu-Cu interactions. On RuB, the preference, by only 0.10 eV, is for Cu atoms to migrate away from each other with one atom anchored at the Ru site.

To summarize, the doping of Ru in TaN surface improves the binding strength of Cu and increases the activation energies for on-surface Cu migration as compared to bare TaN surfaces. We also find that the activation energy to migrate toward the Ru site is smaller than the activation energy to migrate away from it suggesting that the Ru dopants can act as anchor points during copper nucleation. However, the computed activation energies appear to be sensitive to the location of the doping site, therefore, additional calculations are needed where a sufficiently large surface with high percentage of doping is employed, which we plan to address in a subsequent paper.

4 Discussion

Cheng and co-workers[28] laid down three critical conditions for the selection of an ideal liner material for copper electroplating. For the Cu/Ru/TaN system these conditions are as follows: i) adhesion of Cu on Ru must be stronger than on TaN, ii) adhesion of Ru on TaN must be stronger than that of Cu on TaN and iii) adhesion of Ru on TaN must be stronger than that of Cu on Ru.

From our investigation that compared the interactions of one

Cu/Ru adatom on low-index ε-TaN surfaces, we found that the Ru adatom binds about 1.6 to 1.9 times stronger than the Cu adatom. On average, the Cu and Ru atoms adsorbed with a binding energy of -2.57 eV and -4.95 eV, respectively. Complementing the above, the Ru adatom was found to have greater average activation energy for on-surface diffusion (1.02 eV) as compared to the Cu adatom (0.73 eV). Based on the above results we find that condition ii) is satisfied. The average binding energy of Cu on Ru(0 0 1) surface is -3.16 eV, which is about 0.59 eV stronger than Cu binding on the TaN surfaces and about 1.79 eV weaker than Ru binding on TaN. Therefore, all the three conditions laid out by Cheng and coworkers[28] are satisfied for the Cu/Ru/ε-TaN system establishing Ru as an ideal liner/glue material for the Cu-ε-TaN interface as well.

From the two adatom adsorption calculations on the TaN surfaces, we found that the Cu and Ru adatoms bind with an average binding energy of -2.85 eV and -5.02 eV, which are 0.28 eV and 0.07 eV stronger than the one adatom cases, respectively. The additional binding energy comes from either the M-M (M = Cu, Ru) interaction and/or the associated surface relaxations/rearrangements. From activation energy for two atom association on the TaN surfaces, we found that the Cu atoms would associate with lower activation energy than the Ru atoms except in the case of (1 1 1) surface where the activation energies were almost comparable.

The (1 1 0) surface of ε-TaN, with the most favourable surface energy among the low index surfaces, behaved differently from the (1 1 1) and (1 0 0) surfaces in two aspects. Firstly, the Cu and Ru adatoms bound comparatively strongly at the (1 1 1) and (1 0 0) surfaces as compared to the (1 1 0) surface. Secondly, the Cu and Ru adatoms were oxidized on the (1 1 0) surface while they were reduced on the (1 1 1) and (1 0 0) surfaces. This is probably because of the significant difference in the Ta/N charges and coordination geometry in the top layer of these surfaces. The Ta atoms in the first layer of the (1 1 0) surface were more oxidized than those on the other two surfaces which allowed subsequent oxidation of the Cu/Ru atoms on this surface by reduction of the Ta atoms. Moreover, the largest two atom association activation energy for both Ru and Cu was found on the (1 1 0) surface along with significantly reduced activation energy for the reverse process (to keep them separated), therefore this surface was chosen for further analysis concerning Ru passivation and doping.

It is important to note that the on-surface diffusion of Cu adatoms on bare Ru(0 0 1) surface is more favourable, along with significantly lower two atom association activation energies, than on the bare TaN surfaces. If a thick layer of Ru is passivated on the TaN surface, then the deposited copper atoms might diffuse and associate easily and could result in islands of Cu instead of a film. Therefore we first tested the copper activity on 1 ML and 2 ML of Ru passivated TaN surfaces where the hexagonal close packing arrangement of the Ru atoms was already visible. The average adsorption energy of a Cu adatom was very similar (-3.29 eV - 3.34 eV) on these surfaces and was comparable to, if not slightly larger, that on the bare Ru(0 0 1) surface. However, the average computed activation energy for on-surface Cu diffusion was about 0.31 eV on the passivated surfaces which is more favourable than

on the bare Ru(0 0 1) surface, but considerably less favourable than on the bare TaN(1 1 0) surface. This activation energy of 0.31 eV would be easily breached under process temperatures, so we can expect very mobile Cu adatoms on Ru passivated TaN surfaces as well. From the 2 Cu adsorption calculations, we saw that the copper atoms preferred to associate on these surfaces. The average energy needed to separate these associated copper atoms was found to decrease from 0.42 eV in the 1 ML case to 0.25 eV in the 2 ML case. Therefore, 1 ML Ru passivated TaN surface is better at preventing association than the 2 ML of Ru passivated surface which would give a thinner barrier+liner film.

The average sub-surface adsorption energies of a Cu adatom was -2.78 eV and -2.22 eV for the 1 and 2 ML of Ru passivated surfaces, respectively, which are significantly more favourable than on the bare Ru(0 0 1) surface (-1.79 eV). This is accompanied by the fact that the average activation energy for the exchange of Cu and Ru atoms is about 0.86 eV and 1.83 eV for the 1 and 2 ML of Ru passivated surfaces, which are almost twice as low as that on the bare Ru(0 0 1) surface (2.98 eV). So the sub-surface diffusion of Cu adatoms through the Ru layer via exchange process is more probable on the Ru passivated surfaces than the bare Ru. The activation energy for this exchange mechanism will probably increase when more layers of Ru are considered. Based on the above evidence, passivation of TaN surfaces with Ru may not be the best solution there is to avoid Cu association and enhance Cu binding. As an alternative, we looked at Ru doped TaN surfaces which would also reduce the overall layer thickness.

We considered two Ru doped TaN (1 1 0) surfaces where a S or F type surface Ta atom is replaced by a Ru atom (RuA or RuB). The RuB doped surface is energetically more favourable than the RuA doped surface and the RuA atom is more oxidized than the RuB. The Ru doping does not introduce significant changes in the surface lattice as well as surface charge distribution. Differences, if any, are small and localized to the doping site. Overall the Cu binding energy is more favourable when Ru is present in the TaN (1 1 0) surface, more so when the Cu atom is bound to the doped Ru. The Cu binding energies and the surface geometry did not change with a larger surface supercell, which also suggested that the effect of Ru doping is local. The average 1 Cu binding energy on the Ru doped surface is about -2.46 eV, which is 0.86 eV weaker than that on the Ru passivated surfaces. However, the adsorption energies were significantly decreased to an average of -2.88 when 2 Cu atoms are adsorbed due to the increased Cu-Ru and Cu-Cu binding. On the other hand, the on-surface diffusion of Cu atoms and two atom association are considerably hindered on the Ru doped surfaces as compared to the Ru passivated surfaces. In fact, the two atom association activation energies on the doped surfaces are comparable to that of bare TaN surface. Further, the sub surface adsorption and diffusion of the Cu atoms are also comparatively less favourable on the Ru doped surfaces as compared to the Ru passivated surfaces. We also showed that the migration of Cu towards the doped Ru is more favourable than the migration away from it. This suggested clearly that the Ru binding sites can be anchor points for Cu nucleation during the initial stages of the deposition process. Therefore, a higher percentage of Ru doping would ensure that the Cu atoms do not associate on the surface.

In any case additional calculations on much larger surface models are needed to confirm the above, which will be addressed in our next paper.

Compared to the Ru passivated surfaces where the Cu atoms diffuse and associate easily despite the more favourable binding of Cu, the Ru doped surfaces provide smaller activation energies toward diffusion and association of the adsorbed Cu atoms. Moreover, the Cu binding energies on the Ru doped surfaces are more favourable as compared to bare TaN surfaces and we expect further improvements as the percentage of Ru doping is increased. Therefore, we find that the Ru doped surfaces exhibit a great potential as a combined barrier+liner material, as the addition of Ru modifies the TaN surface to give increased binding and provide anchoring sites for the Cu nucleation, which should promote wetting of Cu while retaining the barrier properties of TaN.

5 Conclusions

We have investigated the viability of Ru passivated and Ru doped ε-TaN surfaces as an effective diffusion barrier+liner material for copper interconnect technology. We started by studying the activity of Cu and Ru adatoms on bare ε-TaN surfaces and found that Ru binds significantly stronger and diffuses slower than Cu. Cu was found to bind at the Ru(0 0 1) surface with roughly the same average binding energy as at the TaN surfaces, however, Cu diffused faster on the Ru surface. On-surface association and sub-surface adsorption of Cu atoms were relatively more favourable at the Ru(0 0 1) surface. Therefore, several monolayers of Ru deposited on TaN can not be considered as the most effective barrier+liner material.

TaN (1 1 0) surface was chosen for the Ru passivation and doping studies since both Ru and Cu adatoms did not prefer to associate on it as compared to (1 1 1) and (1 0 0) surfaces. On the Ru passivated (1 1 0) surfaces, Cu atoms bind more strongly than on the bare TaN and Ru surfaces. However, the adsorbed Cu atoms diffused faster than on the bare TaN surfaces and preferred to associate. Although 1 or 2 ML of Ru passivation on TaN was a better alternative to several layers of Ru on TaN, it still lacks the association behaviour that we are expecting in the combined barrier+liner material. Finally, we looked at Ru doped TaN surface as a viable alternative. On the Ru doped surfaces, even though the Cu adatoms showed decreased Cu binding as compared to the Ru passivated surfaces, they offered significantly larger activation energies for the on-surface and sub-surface diffusion as well as association of Cu atoms. We also expect the Cu binding to improve at higher percentage of Ru doping. Therefore we find the Ru doped TaN surfaces to be a promising combined barrier+liner material which incorporates both the liner properties of Ru and barrier properties of TaN.

Conflicts of interest

There are no conflicts to declare.

Acknowledgements

Notes and references

1 P. S. Peercy, *Nature*, 2000, **406**, 1023–1026.

2 M. T. Bohr, *Int. El. Devices Meet.*, 1995, 241–244.

3 K. N. Tu, *J. Appl. Phys.*, 2003, **94**, 5451–5473.

4 B. Li, C. Christiansen, D. Badami and C.-C. Yang, *Microelectron. Reliab.*, 2014, **54**, 712–724.

5 S.-Q. Wang, *MRS Bull.*, 1994, **19**, 30–40.

6 D. C. Edelstein, *Int. El. Devices Meet.*, 2017, 14.1.1–14.1.4.

7 Z. Wang, T. Ida, H. Sakaue, S. Shingubara and T. Takahagi, *Electrochem. Solid St.*, 2003, **6**, C38–C41.

8 B. Pesic, *ECS Transactions*, 2007, **2**, 243–256.

9 H. Wong, N. M. Shukor and N. Amin, *Microelectron. J.*, 2007, **38**, 777–782.

10 A. E. Kaloyeros and E. Eisenbraun, *Annu. Rev. Mater. Sci.*, 2000, **30**, 363–385.

11 M. Uekubo, T. Oku, K. Nii, M. Murakami, K. Takahiro, S. Yamaguchi, T. Nakano and T. Ohta, *Thin Solid Films*, 1996, **286**, 170–175.

12 K. Holloway and P. M. Fryer, *Appl. Phys. Lett.*, 1990, **57**, 1736–1738.

13 H. Kim, Y. Naito, T. Koseki, T. Ohba, T. Ohta, Y. Kojima, H. Sato and Y. Shimogaki, *Jpn. J. Appl. Phys.*, 2006, **45**, 2497–2501.

14 O. Chyan, T. N. Arunagiri and T. Ponnuswamy, *J. Electrochem. Soc.*, 2005, **150**, C347–C350.

15 T. N. Arunagiri, Y. Zhang, O. Chyan, M. El-Bouanani, M. J. Kim, K. H. Chen, C. T. Wu and L. C. Chen, *Appl. Phys. Lett.*, 2005, **86**, 083104-1–083104-3.

16 N. Torazawa, S. Hirao, S. Kanayama, H. Korogi and S. Matsumoto, *J. Electrochem. Soc.*, 2016, **163**, E173–E178.

17 K. Min, K. Chun and K. Kim, *J. Vac. Sci. Technol. B*, 1996, **14**, 3263–3269.

18 Y. Zhao and G. Lu, *Phys. Rev. B*, 2009, **79**, 214104-1–214104-9.

19 K.-C. Park and K.-B. Kim, *J. Electrochem. Soc.*, 1995, **142**, 3109–3115.

20 K. S. Novoselov, D. Jiang, F. Schedin, T. J. Booth, V. V. Khotkevich, S. V. Morozov and A. K. Geim, *P. Natl. Acad. Sci.*, 2005, **102**, 10451–10453.

21 W. Choi, N. Choudhary, G. H. Han, J. Park, D. Akinwande and Y. H. Lee, *Mater. Today*, 2017, **20**, 116–130.

22 C. Lo, K. Zhang, J. A. Robinson and Z. Chen, *2018 Int. Symp. VLSI Technol., Sys. Appl. (VLSI-TSA)*, 2018, 1–2.

23 D. V. Greenslit and E. Eisenbraun, *ECS Transactions*, 2011, **35**, 17–24.

24 S. M. George, *Chem. Rev.*, 2010, **110**, 111–131.

25 K. J. Kanarik, T. Lill, E. A. Hudson, S. Sriraman, S. Tan, J. Marks, V. Vahedi and R. A. Gottscho, *J. Vac. Sci. Technol. A*, 2015, **33**, 020802-1–020802-14.

26 Z. Wu, R. Li, X. Xie, W. Suen, J. Tseng, N. Bekiaris, R. Vinnakota, K. Kashefizadeh and M. Naik, *2018 Int. Interconnect Technology Conf. (IITC)*, 2018, 149–151.

27 M. Stavrev, D. Fischer, F. Praessler, C. Wenzel and K. Drescher, *J. Vac. Sci. Technol. A*, 1999, **17**, 993–1001.

28 B. Han, J. Wu, C. Zhou, B. Chen, R. Gordon, X. Lei, D. A. Roberts and H. Cheng, *Angew. Chem. Int. Edit.*, 2010, **49**, 148–152.

29 S.-F. Ding, H.-S. Lu, F. Chen, Y.-L. Jiang, G.-P. Ru, D. W. Zhang and X.-P. Qu, *Jpn. J. Appl. Phys.*, 2011, **50**, 105701-1–105701-5.

30 K. Frisk, *J. Alloy. Compd.*, 1998, **278**, 216–226.

31 A. Christensen and B. Lebech, *Acta Crystallogr. B*, 1978, **34**, 261–263.

32 N. C. Hernandez, A. Marquez, J. F. Sanz, J. R. B. Gomes and F. Illas, *J. Phys. Chem. B*, 2004, **108**, 15671 – 15678.

33 A. D. Vitto, G. Pacchioni, F. O. Delbecq and P. Sautet, *J. Phys. Chem. B*, 2005, **109**, 8040–8048.

34 L. Giordano, M. Baistrocchi and G. Pacchioni, *Phys. Rev. B*, 2005, **72**, 115403-1–115403-12-.

35 M. Nolan, S. D. Elliott, J. S. Mulley, R. A. Bennett, M. Basham and P. Mulheran, *Phys. Rev. B*, 2008, **77**, 235424-1–235424-11.

36 M. Nolan, *J. Chem. Phys.*, 2012, **136**, 134703-1–134703-9.

37 W. Q. Li, S. G. Srinivasan, D. R. Salahub and T. Heine, *Phys. Chem. Chem. Phys.*, 2016, **18**, 11139–11149.

38 H. Pinto, V. Haapasilta, M. Lokhandwala, S. Oberg and A. S. Foster, *J. Phys.: Condens. Matter*, 2017, **29**, 135001-1–135001-5.

39 N. J. O'Connor, A. S. M. Jonayat, M. J. Janik and T. P. Senftle, *Nat. Catal.*, 2018, **1**, 531–539.

40 I. A. Pasti, B. Johansson and N. V. Skorodumova, *Phys. Chem. Chem. Phys.*, 2018, **20**, 6337–6346.

41 Y. Chen, S. Ji, C. Chen, Q. Peng, D. Wang and Y. Li, *Joule*, 2018, **2**, 1242–1264.

42 N. Dimakis, I. Salas, L. Gonzalez, O. Vadodaria, K. Ruiz and M. I. Bhatti, *Molecules*, 2019, **24**, 754-1–754–28.

43 G. Kresse and J. Furthmuller, *Phys. Rev. B*, 1996, **54**, 11169–11186.

44 P. Blochl, *Phys. Rev. B*, 1994, **50**, 17953–17979.

45 G. Kresse and D. Joubert, *Phys. Rev. B*, 1999, **59**, 1758–1775.

46 J. P. Perdew, K. Burke and M. Ernzerhof, *Phys. Rev. Lett.*, 1996, **77**, 3865–3868.

47 G. Henkelman and H. Jonsson, *J. Chem. Phys.*, 2000, **113**, 9978–9985.

48 G. Henkelman, B. P. Uberuaga and H. Jonsson, *J. Chem. Phys.*, 2000, **113**, 9901–9904.

49 K. Persson, *Materials Data on TaN by Materials Project*, 2015, URL: https://materialsproject.org/materials/mp-1279/, accessed on 21/11/2018.

50 E. Sanville, S. D. Kenny, R. Smith and G. Henkelman, *J. Comput. Chem.*, 2007, **28**, 899–908.

51 G. Henkelman, A. Arnaldsson and H. Jónsson, *Comp. Mater. Sci.*, 2006, **36**, 354–360.

52 K. Persson, *Materials Data on Ta by Materials Project*, 2016, URL: https://materialsproject.org/materials/mp-50/, accessed on 21/11/2018.

53 A. Hjorth Larsen, J. J. Mortensen, J. Blomqvist, I. E. Castelli, R. Christensen, M. Dulak, J. Friis, M. N. Groves, B. Hammer, C. Hargus, E. D. Hermes, P. C. Jennings, P. B. Jensen, J. Kermode, J. R. Kitchin, E. L. Kolsbjerg, J. Kubal, K. Kaasbjerg, S. Lysgaard, J. B. Maronsson, T. Maxson, T. Olsen, L. Pastewka, A. Peterson, C. Rostgaard, J. Schiotz, O. Schutt, M. Strange, K. S. Thygesen, T. Vegge, L. Vilhelmsen, M. Walter, Z. Zeng and K. W. Jacobsen, *J. Phys-condens. Mat.*, 2017, **29**, 273002-1–273002-30.

54 K. Persson, *Materials Data on Ru by Materials Project*, 2016, URL: https://materialsproject.org/materials/mp-33/, accessed on 21/11/2018.

55 J. W. Arblaster, *Platin. Met. Rev.*, 2013, **57**, 127–136.

56 E. Kaxiras, *Atomic and Electronic Structure of Solids*, Cambridge University Press, 2003.

57 S.-F. Ding, S.-R. Deng, H.-S. Lu, Y.-L. Jiang, G.-P. Ru, D. W. Zhang and X.-P. Qu, *J. Appl. Phys.*, 2010, **107**, 103534-1–103534-7.